Global Conformation of the *Escherichia coli* Replication Factor DnaC Protein in Absence and Presence of Nucleotide Cofactors†

Roberto Galletto, Rodrigo Maillard, Maria J. Jezewska, and Wlodzimierz Bujalowski*

Department of Human Biological Chemistry and Genetics, Department of Obstetrics and Gynecology, the Sealy Center for Structural Biology, Sealy Center for Cancer Cell Biology, The University of Texas Medical Branch at Galveston, 301 University Boulevard, Galveston, Texas 77555-1053

Received March 31, 2004; Revised Manuscript Received June 3, 2004

ABSTRACT: Global conformational and oligomeric states of the *Escherichia coli* replicative factor DnaC protein in the absence and presence of magnesium and nucleotide cofactors, ATP and ADP, and their fluorescent analogues, MANT-ATP and MANT-ADP, have been examined using analytical sedimentation velocity and time-dependent fluorescence anisotropy techniques. In solution, the DnaC protein exists exclusively as a monomer over a large protein concentration range. The value of $s^{\circ}_{20,w} = 2.45 \pm 0.07$ S indicates that the protein molecule has an elongated shape. When modeled as a prolate ellipsoid of revolution, the hydrated DnaC protein has an axial ratio of 4.0 ± 0.6 with long axis $a = 112$ Å and the short axis $b = 28$ Å, respectively. The presence of magnesium or nucleotide cofactors, ATP or ADP, does not affect the global conformation of the protein and its monomeric state. These data indicate that recently found cooperative interactions between the DnaC molecules, in the complex with the DnaB helicase, are induced by the binding to the helicase, i.e., they are not the intrinsic property of the DnaC protein. Fluorescence anisotropy decays of the DnaC−MANT-ATP and DnaC−MANT-ADP complexes indicate that the protein has a rigid global structure on the nanosecond time scale, little affected by the nucleotide cofactors. Nevertheless, the complex with ATP has a more flexible structure, while the complex with ADP is more rigid, with the protein molecule assuming a more elongated shape. Magnesium exerts control only on the complex with the ATP analogue. In the absence of magnesium, the ATP analogue is firmly held in the binding site. In the presence of Mg^{2+}, this fixed location is released and the analogue is allowed to assume a flexible conformational state. The significance of the results for the functioning of the DnaC protein is discussed.

The DnaC protein is an essential replication protein in the *Escherichia coli* cell that participates in the formation of the replication fork as well as in the assembly of the primosome, a multiprotein−DNA complex that can translocate along the DNA, while synthesizing short oligoribonucleotide primers that are used to initiate synthesis of the complementary strand (*1*−*3*). Mutational analyses indicate that the protein is involved in initiation and elongation stages of the chromosomal DNA replication (*5*, *6*). The role of the DnaC protein in these processes is thought to be strictly related to the specific binding to the *E. coli* primary replicative helicase, the DnaB protein, in the presence of ATP (*1*−*7*). Because the DnaC protein is not necessary for the DnaB helicase to bind the ssDNA, formation of the DnaC−DnaB−ATP/ADP complex must allow the helicase to recognize the specific protein−nucleic acid complex formed at the replication origin (oriC) (*8*). The DnaC protein is absolutely required for this recognition (*9*−*11*).

Thermodynamic studies showed that the DnaC protein has a single nucleotide-binding site, highly specific for the adenine base (*12*). Binding of nucleotides containing bases different than adenine has not been detected. In the presence of magnesium, both ATP and ADP have the same affinity for the nucleotide-binding site of the DnaC protein. However, in the absence of Mg^{2+} cations there are significant differences in interactions between the ATP and ADP cofactors and the DnaC protein, both in the structure of the formed complexes and in the affinities. The affinity of the ATP analogue is lower by a factor of ∼6 than in the presence of magnesium. On the other hand, the binding constant of MANT-ADP is increased by a factor of ∼2, as compared to the value determined in the presence of Mg^{2+}. The obtained data indicate that the complexes of the DnaC protein with nucleotide cofactors are specifically controlled by magnesium binding to the protein, through allosteric interactions between the magnesium and the nucleotide-binding site (*12*−*14*).

In light of the essential role of the DnaC protein in the *E. coli* cell replication, it is surprising that very little is known about the structure of the DnaC protein and its complexes with nucleotide cofactors. Kinetic analyses of binding of the fluorescent nucleotide analogues, MANT-ATP and MANT-ADP, to the DnaC protein indicate that the DnaC protein exists in a preequilibrium conformational transition prior to the nucleotide binding (*12*−*14*). The nucleotide cofactors

† This work was supported by NIH Grant GM-46679 (to W.B.).

* Corresponding author: Dr. W. M. Bujalowski. Department of Human Biological Chemistry & Genetics. The University of Texas Medical Branch at Galveston. Tel: (409) 772-5634. Fax: (409) 772−1790. E-mail: wbujalow@utmb.edu.

[1] Abbreviations: ATP, adenosine 5′-triphosphate; ADP, adenosine 5′-diphosphate; MANT-ATP, 3′-*O*-(*N*-methylantraniloyl)-5′-triphosphate; MANT-ADP, 3′-*O*-(*N*-methylantraniloyl)-5′-diphosphate; Tris, tris(hydroxymethyl)aminomethane; DTT, dithiothreitol.

10.1021/bi049377y CCC: $27.50
Published on Web 08/04/2004

bind to only one of the protein conformations. Moreover, both MANT-ATP and MANT-ADP bind to the same protein conformation in a two-step sequential process in which the bimolecular reaction is followed by a single conformational transition of the formed protein−nucleotide complex. Although recent studies show that the DnaC interactions with the helicase are independent of the nucleotide binding to the DnaC protein, the fact that the protein and ATP are absolutely required for the initiation of replication strongly suggest that structural elements of the DnaC protein are specifically recognized by the fork apparatus (*8*).

Elucidation of the structure of the DnaC protein and its complexes with magnesium and nucleotide cofactors is of paramount importance for our understanding of the activities of this essential replication factor. There are several questions that should be addressed. What is the dominant oligomeric state of the protein in solution and how it is affected by magnesium and nucleotide cofactors? Are there significant global structural differences between the two DnaC conformations prior to the nucleotide binding? Is magnesium affecting the conformational equilibrium? How does the complex of the DnaC protein with ATP differ from the complex with ADP in the presence and absence of Mg^{2+} cations? The binding of six DnaC molecules to the DnaB hexamer is characterized by positive cooperativity (*15*). Are the cooperative interactions an intrinsic property of the DnaC protein or are they exclusively induced by interactions with the helicase?

In this communication, we examine the global structure of the DnaC protein and its complexes with magnesium, ATP, and ADP, using the analytical sedimentation velocity and time-dependent fluorescence anisotropy techniques. We obtain evidence that the protein is exclusively in a monomeric state independently of the examined solution conditions. The DnaC molecule in solution has an elongated shape and, when modeled as a prolate ellipsoid of revolution, has an axial ratio of 4 ± 0.6. Binding of magnesium or nucleotide cofactors has little effect on the global conformation of the protein and its monomeric state. The global structure of the DnaC protein is rigid in the nanosecond time scale. Nevertheless, the data strongly suggest that the protein has more flexible structure in the presence of ATP than ADP.

MATERIALS AND METHODS

Reagents and Buffers. All chemicals were reagent grade. All solutions were made with distilled and deionized 18 MΩ (Milli-Q) water. The standard buffer, T4, is 50 mM Tris adjusted to pH 8.1 at appropriate temperatures with HCl, 10% glycerol, and 1 mM DTT. The temperature and concentrations of salt in the buffer are indicated in the text.

Nucleotides. MANT-ATP and MANT-ADP were synthesized as described before (*16*−*21*). The concentrations of the nucleotides were spectrophotometrically determined, using the extinction coefficient $\epsilon_{356} = 5800\ M^{-1}\ cm^{-1}$.

DnaC Protein. The *E. coli* DnaC protein was purified as previously described by us (*12*−*14*). The concentration of the protein was spectrophotometrically determined using the extinction coefficient $\epsilon_{280} = 2.32 \times 10^4\ M^{-1}\ cm^{-1}$ determined using a method based on Edelhoch's approach (*22*, *23*).

Steady-State Fluorescence Measurements. All fluorescence measurements were performed using Fluorolog-3 (Jobin Yvon-SPEX, Edison, NJ) spectrofluorometer, as previously described by us (*18*−*21*). The binding was followed by monitoring the fluorescence of nucleotide analogues ($\lambda_{ex} =$ 356 nm, $\lambda_{em} = 450$ nm) as described before (*18*−*21*).

Time-Dependent Fluorescence Measurements. Time-dependent fluorescence lifetime and anisotropy measurements have been performed using an IBH 5000U time-correlated single photon counting instrument (IBH, Glasgow, UK) equipped with polarizers as well as excitation and emission monochromators. Excitation of the MANT residue at 370 nm was performed with a nanosecond light emitting laser diode with emission recorded at 450 nm. At least ~10 000 counts were collected at the peak with vertical orientation of both polarizers with respect to the direction of the light beam. Glycogen solution was used as a reference for the excitation source profile. The total emission of the sample is defined as $F_{Tot} = I_{VV} + 2GI_{VH}$, where I_{VV} is the fluorescence intensity and the first and second subscripts refer to vertical (V) polarization of the excitation and vertical (V) or horizontal (H) polarization of the emitted light. The factor $G = I_{HV}/I_{HH}$ corrects for the different sensitivity of the emission monochromator for vertically and horizontally polarized light (*24*, *25*). Deconvolution analyses of total fluorescence emission decay curves were performed using the nonlinear, least-squares software provided by the manufacturer, with the exponential function defined as

$$F_{Tot}(t) = I_{VV}(t) + 2GI_{VH}(t) = \sum_{i=1}^{n} A_i \exp(-t/\tau_i) \quad (1)$$

where $F(t)$ is the fluorescence intensity at time t, A_i is the amplitude corresponding to the ith decay process, τ_i is the fluorescence lifetime characterizing the ith decay process, and n is the number of decay processes. Analyses of fluorescence anisotropy decays were performed by deconvolution of the difference function, $d(t)$, defined as (*25*)

$$d(t) = I_{VV}(t) - I_{VH}(t) = \left[\sum_{i=1}^{n} A_i \exp(-t/\tau_i)\right]\left[\sum_{i=1}^{m} r_i \exp\left(-\frac{t}{\tau_{Ci}}\right)\right] + b \quad (2)$$

and by directly fitting the anisotropy function

$$r(t) = \frac{I_{VV}(t) - I_{VH}(t)}{I_{VV}(t) + 2GI_{VH}(t)} = \sum_{i=1}^{m} r_i \exp\left(-\frac{t}{\tau_{Ci}}\right) + b \quad (3)$$

where b is the corresponding baseline correction and m is the number of rotational correlation times.

Analytical Ultracentrifugation Measurements. Sedimentation velocity experiments were performed with an Optima XL-A analytical ultracentrifuge (Beckman Inc., Palo Alto, CA) using double-sector charcoal-filled 12-mm centerpieces as we described previously (*15*, *26*−*28*). Sedimentation velocity scans were collected at the absorption band of the DnaC protein at 280 nm. The DnaC−nucleotide complexes were scanned at 290 nm where the cofactor absorbance is minimal and the absorbance of the sample is dominated by the protein. Time derivative analyses of sedimentation scans were performed with the software supplied by the manufacturer using averages of 8−15 scans for each concentration

as described before (*15*, *29*, *30*). The values of sedimentation coefficients were corrected to $s_{20,w}$ for solvent viscosity and temperature to standard conditions (*31*).

RESULTS

Analytical Sedimentation Velocity Studies of the DnaC Protein in the Absence and Presence of Magnesium and Nucleotide Cofactors, ATP, or ADP. Analytical sedimentation technique provides direct information about the hydrodynamic properties of a macromolecule, reflecting its global conformational properties (*31*, *32*). The sedimentation velocity profiles (monitored at 280 nm) of the DnaC protein in buffer T4 (pH 8.1, 20 °C), containing 100 mM NaCl, in an absence of magnesium, are shown in Figure 1a. The concentration of the protein is 9.76×10^{-5} M and the sedimentation run has been performed at 60 000 rpm. Inspection of the profiles clearly shows that there is a single moving boundary. Similar experiments have been performed in the presence of 5 mM $MgCl_2$ (data not shown). To obtain the sedimentation coefficient of the protein, sedimentation scans have been analyzed using the time-derivative approach as we described before (*15*). The advantages of time-derivative approach over the traditional moment method are thoroughly discussed in the literature (*29*, *30*).

The dependence of the sedimentation coefficient of the DnaC protein upon the protein concentration, obtained in the absence and presence of magnesium, is shown in Figure 1b. The value of $s_{20,w}$ shows, within the experimental accuracy, very little, if any, dependence upon [DnaC] in the examined protein concentration range. The same behavior is observed in the presence of Mg^{2+} (Figure 1b). Analogous sedimentation velocity studies have been performed in the presence of the ATP and ADP. The dependence of the sedimentation coefficient of the DnaC protein upon the protein concentration, in buffer T4 (pH 8.1, 20 °C), containing 100 mM NaCl and 5 mM $MgCl_2$, obtained in the presence of 0.1 mM ATP or 0.1 mM ADP, are included in Figure 1b. At selected concentrations of ATP and ADP, the DnaC protein is saturated with the cofactors (*12*−*14*). The analogous data in the presence of the cofactors, but obtained in the absence of magnesium, are shown in Figure 1c. In these studies, the reference cell contains the same concentration of the nucleotide cofactor, thus, allowing us to exclusively monitor the absorbance of the protein. The obtained values of $s_{20,w}$ are, within the experimental accuracy, the same as observed for the protein alone and in the presence and absence of magnesium. The extrapolation of the plots to [DnaC] = 0 provides $s^{\circ}_{20,w} = 2.45 \pm 0.07$ S in all examined solution conditions (Figure 1b,c).

There are two important aspects of the data. First, there is a clear lack of any oligomerization process of the DnaC protein over a large range of the [DnaC]. This is true for the protein alone and its complexes with magnesium and nucleotide cofactors. Moreover, the same values of $s_{20,w}$ are obtained in the presence of magnesium, ATP, and ADP. Such behavior indicates that neither the binding of Mg^{2+} cations nor the specific binding of nucleotide cofactors induce global changes in the DnaC protein structure as sensed by translational movement. Second, the same values of $s_{20,w}$ in the presence of ATP and ADP indicate that tri- and diphosphate adenosine nucleotides do not induce detectable and different

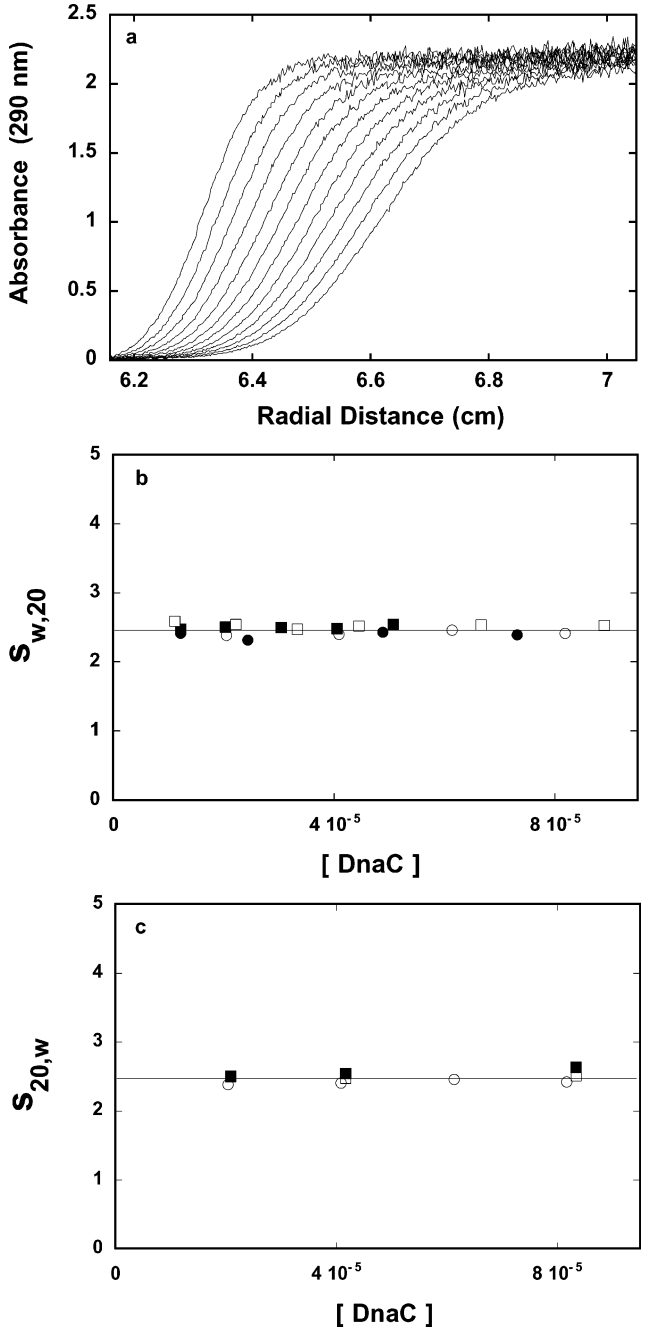

FIGURE 1: (a) Sedimentation velocity absorption profiles at 280 nm of the DnaC protein in buffer T4 (pH 8.1, 10 °C), containing 100 mM NaCl. The concentration of the DnaC protein is 9.76×10^{-5} M; 60 000 rpm. (b) The dependence of the DnaC protein sedimentation coefficient, $s_{20,w}$, upon protein concentration in buffer T4 (pH 8.1, 10 °C) containing 100 mM NaCl (■), 100 mM NaCl and 5 mM $MgCl_2$ (□), 100 mM NaCl, 5 mM $MgCl_2$, and 0.1 mM ATP (●), 100 mM NaCl, 5 mM $MgCl_2$, and 0.1 mM ADP (○). (c) The dependence of the DnaC protein sedimentation coefficient, $s_{20,w}$, upon protein concentration in buffer T4 (pH 8.1, 10 °C) containing 100 mM NaCl (○), 100 mM NaCl and 0.1 mM ATP (■), 100 mM NaCl and 0.1 mM ADP (□). The solid lines in all plots have no theoretical basis and follow the experimental data.

global structure changes in the DnaC protein, independently of the presence of magnesium (see Discussion).

Global Conformation of the DnaC Protein in Solution. Determination of the sedimentation coefficient, $s^{\circ}_{20,w}$, allowed us to evaluate the hydrodynamic properties of the protein (*31*−*33*). The simplest and physically realistic model

of the shape of the protein molecule is that of prolate ellipsoid of revolution (*31*−*33*). The sedimentation coefficient is related to the average, frictional coefficient, $\bar{f}_e$, of the hydrated prolate ellipsoid by

$$s^{\circ}_{20,w} = \frac{M(1 - \bar{\nu}\rho)}{N_A \bar{f}_e} \quad (4)$$

The average translational frictional coefficient, $\bar{f}_e$ of a prolate ellipsoid, is defined by the Perrin equation as (*31*−*33*)

$$\bar{f}_e = \left\{ \frac{\sqrt{p^2 - 1}}{p^{1/3}\{\ln[p + \sqrt{1 - p^2}]\}} \right\} 6\pi\eta R_h \quad (5)$$

where R_h is the hydrodynamic radius of the corresponding hydrated sphere, defined as

$$R_h = \left[\frac{3M(\bar{\nu} + h\bar{\nu}_S)}{N_A 4\pi} \right]^{1/3} \quad (6)$$

where p is the axial ratio of the major ellipsoid axis, a, to the minor one, b, i.e., $p = a/b$, M is the molecular weight of the anhydrous DnaC protein (27876.3) (*34*), N_A is the Avogadro number, $\bar{\nu}$ is the protein partial specific volume, ρ is the density of the solvent in g/mL, η is the viscosity of the solvent (poise), h is the degree of the protein hydration expressed as $g_{H_2O}/g_{protein}$, and $\bar{\nu}_s$ is the partial specific volume of the solvent equal to the inverse of ρ. Partial specific volume of the DnaC protein, $\bar{\nu} = 0.736$ mL/g, was calculated from the amino acid composition of the protein (*35*). The degree of hydration can be estimated by the method of Kuntz (*36*). It provides $h = 0.39\ g_{H_2O}/g_{protein}$. However, this value of h is calculated for the mixture of amino acids completely exposed to water, and it represents a possible maximum value of the degree of hydration for the protein. Part of amino acid residues of the protein will not be accessible to water in the native structure. Thus, the value of the degree of hydration should be corrected for the part of residues in the native structure that is not accessible to the hydration. The correction factor can be obtained in a systematic way by comparing Kuntz's values for a series of proteins, with the hydration values of the folded structure of the same protein (*37*, *38*). The correction factor amounts to 0.7−0.74, thus only ∼70% of the maximum values of h is associated with the folded protein molecule. The corrected value for the DnaC protein is $h = 0.273\ g_{H_2O}/g_{protein}$ (*37*, *38*).

The computer simulation of the sedimentation coefficient of the DnaC protein as a function of the ellipsoid axial ratio, p, using the corrected value of the degree of hydration, h, is shown in Figure 2. The plot has been obtained using eqs 4−6. For comparison, the dependence of the sedimentation coefficient as a function of the axial ratio of the ellipsoid for the completely nonhydrated protein and with maximum degree of hydration, are also included. The value of $s^{\circ}_{20,w} = 2.45 \pm 0.07$ indicates that the DnaC protein in solution, with the corrected degree of hydration, has a nonspherical, asymmetric structure and, when modeled as a prolate ellipsoid, has an apparent axial ratio of $p = 4.0 \pm 0.6$. For the completely nonhydrated and maximum hydrated protein, the same axial ratio would be $p = 6.0 \pm 0.6$ and 3.4 ± 0.5, respectively (Figure 2, see Discussion).

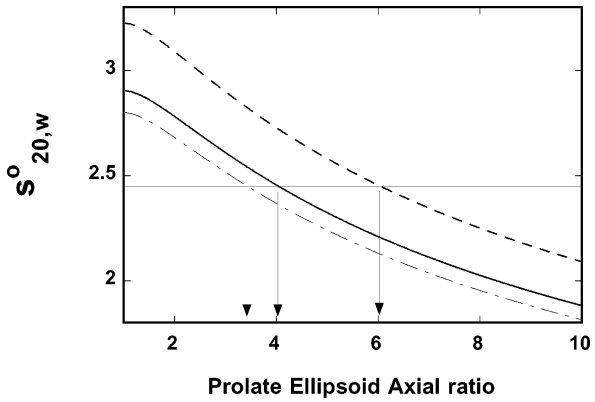

FIGURE 2: Computer simulation of the sedimentation, $s^{\circ}_{20,w}$, as a function of the axial ratio of the prolate ellipsoid of revolution, p, for different values of the degree of hydration, h ($g_{H_2O}/g_{protein}$); 0.39 (− - −), 0.273 (—); 0 (− − −) The plots have been generated using eqs 4−6. The solid horizontal line marks the value of the sedimentation coefficient, $s^{\circ}_{20,w} = 2.45$. The arrows indicate values of the axial ratio, p, corresponding to the same $s^{\circ}_{20,w}$ at different degrees of hydration (see text for details).

Fluorescence Anisotropy Decays of the DnaC−MANT-ATP and DnaC−MANT-ADP Complexes in the Presence of Magnesium. Binding thermodynamics of fluorescent MANT derivative of adenosine nucleotides are indistinguishable from the unmodified cofactors (*12*−*14*). Moreover, binding of MANT-ATP and MANT-ADP to the DNAC protein is characterized by strong increase of the cofactors' fluorescence, providing an excellent signal to monitor the conformational dynamics of the formed complexes. Thus, we address the conformation of the DnaC protein in complexes with the nucleotide cofactors, in the presence of Mg^{2+} cations, using time-dependent fluorescence anisotropy technique (*25*, *39*−*41*).

The decay of the total emission, $F_{Tot}(t)$ of the MANT-ATP in the presence of the DnaC protein ($\lambda_{ex} = 370$ nm, $\lambda_{em} = 450$ nm) in buffer T4 (pH 8.1, 20 °C), containing 100 mM NaCl and 5 mM $MgCl_2$, is shown in Figure 3a. The concentration of the nucleotide and the DnaC protein are 5×10^{-6} and 1.2×10^{-4} M, respectively. At these concentrations, the nucleotide cofactor is virtually completely saturated with the protein (*12*−*14*). The solid line is the nonlinear least-squares fit of the experimental curve, using the two-exponential function (eq 1). As shown by the included residuals, the two-exponential fit provides adequate description of the experimental curve. The total fluorescence intensity of the MANT-ATP bound to the DnaC is characterized by fluorescence lifetimes $\tau_1 = 5.6 \pm 0.3$ and $\tau_2 = 9.9 \pm 0.5$ ns and relative amplitudes $A_1 = 0.16 \pm 0.01$ and $A_2 = 0.84 \pm 0.01$. Analogous fluorescence intensity decay for the MANT-ADP bound to the DnaC protein is shown in Figure 3b. Similar to the MANT-ATP, the decay is adequately described by the two-exponential function with fluorescence lifetimes $\tau_1 = 5.6 \pm 0.3$ and $\tau_2 = 9.2 \pm 0.5$ ns and relative amplitudes $A_1 = 0.15 \pm 0.01$ and $A_2 = 0.85 \pm 0.01$ (Table 1). Thus, the longer lifetime component dominates the decay process for both MANT-ATP and MANT-ADP bound to the DnaC protein, providing the time window to examine the rotational dynamics of the protein.

The decays of the fluorescence intensity of the MANT-ATP bound to the DNAC protein, with the excitation polarizer oriented vertically and the emission polarizer

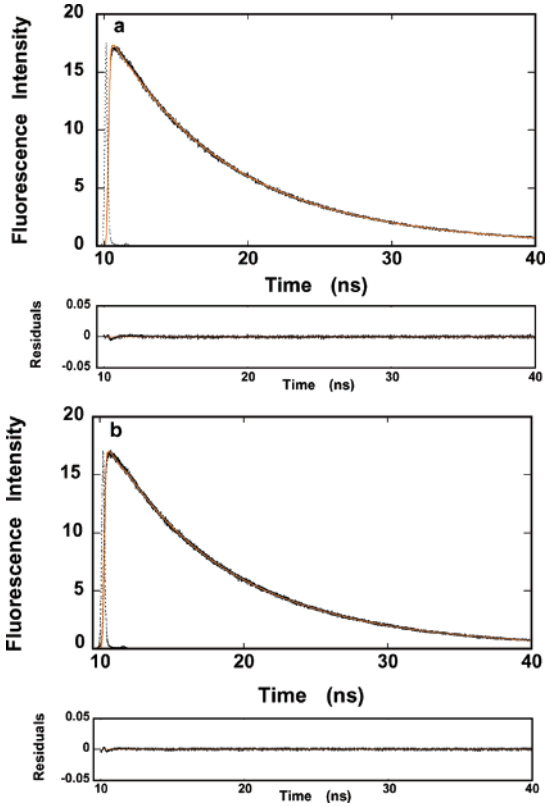

FIGURE 3: (a) Time decay of the total emission of MANT-ATP in the complex with the DnaC protein ($\lambda_{ex} = 370$ nm, $\lambda_{em} = 450$ nm) in buffer T4 (pH 8.1, 20 °C), containing 100 mM NaCl and 5 mM $MgCl_2$. The solid smooth line in the nonlinear least-squares fit of the experimental curve using two-exponential function defined by eq 1, with fluorescence lifetimes $\tau_1 = 5.6$ ns, and $\tau_2 = 9.9$ ns, and corresponding amplitudes $A_1 = 0.16$, $A_2 = 0.84$. (b) Time decay of the total emission of MANT-ADP in the complex with the DnaC protein ($\lambda_{ex} = 370$ nm, $\lambda_{em} = 450$ nm) in buffer T4 (pH 8.1, 20 °C), containing 100 mM NaCl and 5 mM $MgCl_2$. The solid smooth line is the nonlinear least-squares fit of the experimental curve using two-exponential function defined by eq 1, with fluorescence lifetimes $\tau_1 = 5.6$ ns, and $\tau_2 = 9.2$ ns, and corresponding amplitudes $A_1 = 0.15$, $A_2 = 0.85$. The lower panels are residuals of the theoretical curves from the experimental decay traces. The dashed lines are the normalized excitation source profile. In both sets of experimental data, the concentration of the DnaC protein and nucleotide cofactors are 1.2×10^{-4} and 5×10^{-6} M, respectively. The zero time is the time corresponding to the center of the excitation pulse.

oriented vertically, $I_{VV}(t)$, or horizontally, $I_{VH}(t)$, are shown in Figure 4a. The function $I_{VV}(t)$ initially decays fast as a result of fast reorientation of the vertically orientated molecules, while $I_{VH}(t)$ shows initially a slower decay rate as a result of the initial increasing of the population of the horizontally oriented molecules. The difference function, $d(t) = I_{VV}(t) - I_{VV}(t)$, (eq 2) is shown in Figure 4b. The initial value of $d(t)$ decays to ~0 at a longer time regime as a result of averaging of the orientations of the bound MANT-ATP molecules. The solid line in Figure 4b is the nonlinear least-squares fit of the experimental curve to eq 2, deconvoluted with the discrete size of the excitation pulse and using the total fluorescence intensity decay, $F_{Tot}(t)$, depicted in Figure 3a (Materials and Methods). The single-exponential function provides an adequate description of the decay process. Including a higher number of exponents does not significantly improve the statistics of the fit. However, the $r(0)$ that is the limiting value of the anisotropy at $t = 0$, r_{lim}, is only 0.252 ± 0.012 instead of expected $r_o = 0.38 \pm 0.02$ for MANT-ATP at the selected excitation wavelength (*19*). Such low value of r_{lim} indicates that the observed depolarization process is preceded by another very fast process with the rotational correlation time less than ~50 ps, i.e., much shorter than the half width of the excitation pulse (~200 ps). Therefore, the depolarization of the emission of the DnaC−MANT-ATP complex is characterized by two rotational correlation times $\tau_{C1} < 0.05$ ns and $\tau_{C2} = 21.7 \pm 0.5$ ns, with amplitudes, $r_1 = 0.146 \pm 0.005$ and $r_2 = 0.252 \pm 0.012$, respectively (eqs 2 and 3).

It is clear that the rotational mobility of the MANT-ATP−DnaC protein complex, in the presence of magnesium, encompasses two very different processes characterized by rotational correlation times differing by at least a factor of ~400. The first rotational correlation time, $\tau_{C1} < 0.05$ ns, is in the range of picoseconds, i.e., in the range of the rotational correlation time of the free MANT-ATP in solution (data not shown). This value of τ_{C1} strongly suggests that it characterizes the local mobility of the nucleotide cofactor in the binding site or very fast local mobility of the protein surface around the nucleotide-binding site. The fast depolarization process reduces the anisotropy of the system by $r_1 = 0.146 \pm 0.005$ to $r_2 = 0.252 \pm 0.012$, indicating a large reorientation of the nucleotide before the second depolarization process, characterized by $\tau_{C2} = 21.7 \pm 0.5$ ns, significantly affects the observed anisotropy. Contrary to the first depolarization process, the value of τ_{C2} is in the range of tens of nanoseconds indicating that it characterizes the rotational mobility of the entire DnaC protein molecule (*39*−*41*) (see Discussion).

The direct fluorescence anisotropy decay of the MANT-ATP bound to the DnaC, as defined by eq 3, confirms the deconvolution analysis of the difference function, $d(t)$. The time dependence of the fluorescence anisotropy of MANT-ATP, saturated with the DnaC protein, in buffer T4 (pH 8.1, 20 °C), containing 100 mM NaCl and 5 mM $MgCl_2$, is shown in Figure 4c. The anisotropy decay plots have clearly biphasic character indicating the presence of depolarization processes occurring in largely different time ranges. The initial unresolved part of the plot is "slowed" by the discrete size of the excitation pulse (~200 ps); nevertheless, the data

Table 1: Fluorescence Parameters of MANT-ATP and MANT-ADP Nucleotides Bound to the *E. coli* DnaC Protein in Buffer T4 (pH 8.1, 20 °C), Containing 100 mM NaCl, in the Presence and Absence of $MgCl_2$

nucleotide	τ_1 (ns)	τ_2 (ns)	A_1	A_2	r_o	r_{lim}	τ_{C1} (ns)	τ_{C2} (ns)
				5 mM $MgCl_2$				
MANT-ATP + DnaC	5.6 ± 0.3	9.9 ± 0.5	0.16 ± 0.01	0.84 ± 0.01	0.38 ± 0.02	0.252 ± 0.012	<0.05	21.7 ± 0.5
MANT-ADP + DnaC	5.6 ± 0.3	9.2 ± 0.5	0.15 ± 0.01	0.85 ± 0.01	0.38 ± 0.02	0.267 ± 0.012	<0.05	22.8 ± 0.5
				no $MgCl_2$				
MANT-ATP + DnaC	9.5 ± 0.5	13.5 ± 0.5	0.84 ± 0.01	0.16 ± 0.01	0.38 ± 0.02	0.245 ± 0.012	<0.05	46.5 ± 3
MANT-ADP + DnaC	6.8 ± 0.3	9.9 ± 0.5	0.18 ± 0.01	0.82 ± 0.01	0.38 ± 0.02	0.303 ± 0.015	<0.05	22.3 ± 0.5

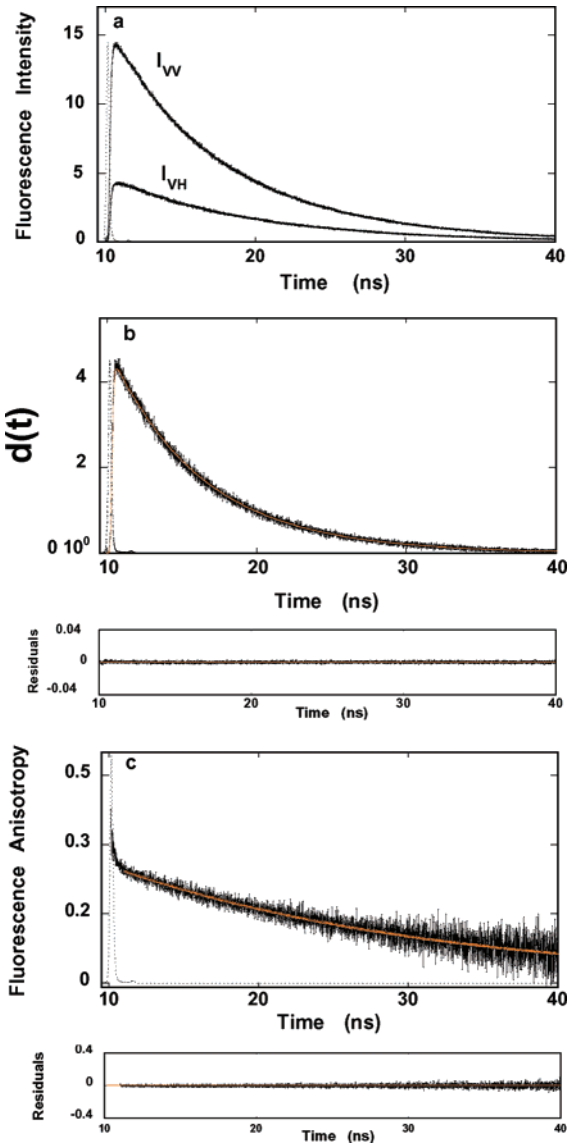

FIGURE 4: (a) Time decays of the MANT-ATP emission in the complex with the DnaC protein (λ_{ex} = 370 nm, λ_{em} = 450 nm) in buffer T4 (pH 8.1, 20 °C), containing 100 mM NaCl and 5 mM $MgCl_2$, with the excitation polarizer oriented vertically and the emission polarizer oriented vertically, $I_{VV}(t)$, and horizontally, $I_{VH}(t)$, respectively. (b) The difference function, $d(t) = I_{VV}(t) - I_{VV}(t)$, as defined by eq 2, obtained from the traces shown in panel a. The solid smooth line is the nonlinear least-squares fit of the experimental curve using the one-exponential function defined by eq 2, deconvoluted with the discrete size of the excitation pulse, with a rotational correlation time τ_{C2} = 21.7 ns, and corresponding anisotropy amplitudes r_2 = 0.252. (c) Time dependence of the MANT-ATP fluorescence anisotropy in the complex with the DnaC protein (λ_{ex} = 370 nm, λ_{em} = 450 nm) in buffer T4 (pH 8.1, 20 °C), containing 100 mM NaCl and 5 mM $MgCl_2$. The solid smooth line is the nonlinear least-squares fit of the experimental curve using eq 3 with a single rotational correlation time τ_{C2} = 21.7 ns, and corresponding anisotropy amplitudes r_2 = 0.241. The G factor at the applied emission wavelength is 0.663. The dashed lines in all panels are the normalized excitation source profiles. The concentration of the DnaC protein and MANT-ATP are 1.2×10^{-4} and 5×10^{-6} M, respectively. The zero time is the time corresponding to the center of the excitation pulse.

indicate that, in the complex, a very fast fluorescence depolarization of the MANT-ATP fluorescence occurs within the time range shorter than one nanosecond. In the time range above ~1 ns, the depolarization occurs at a much slower rate. The solid line in Figure 4c is the nonlinear least-squares fit of the experimental curve, in range above ~2 ns, using single-exponential function defined by eq 3. The theoretical line provides an adequate fit for experimental curve (Figure 4c). The obtained values of the rotational correlation times and anisotropy amplitude of the decay process are $\tau_{C2} = 21.7 \pm 0.5$ ns and $r_2 = 0.241 \pm 0.01$, respectively. Thus, the correlation time and the amplitude, characterizing the time region in which the effect of the pulse duration is negligible, are, within the experimental accuracy, the same as determined from the deconvolution analysis of the difference function (Figure 4b,c).

The analogous decays of the fluorescence intensities, $I_{VV}(t)$ and $I_{VH}(t)$, of the MANT-ADP bound to the DnaC protein are shown in Figure 5a. The difference function, $d(t)$, is shown in Figure 5b. The solid line is the nonlinear least-squares fit of the experimental curve (eq 2) deconvoluted with the discrete size of the excitation pulse and with the total fluorescence intensity decay, $F_{Tot}(t)$ (Figure 4b). The anisotropy decay process is described by single-exponential function with rotational correlation time $\tau_{C2} = 22.8 \pm 0.5$ ns and amplitude $r_2 = 0.267 \pm 0.012$, respectively (Table 1). Similar to the MANT-ATP complex, the value of the anisotropy amplitude is significantly lower than $r_o = 0.38 \pm 0.02$ (see above). Thus, the rotational mobility of the MANT-ADP bound to the DnaC protein encompasses the same two processes differing at least by a factor of ~400 in their rotational correlation times. Figure 5c shows the time dependence of the fluorescence anisotropy of MANT-ADP−DnaC complex. The solid line in Figure 5c is nonlinear least-squares fit of the experimental curve, in the range above 2 ns, using single-exponential function defined by eq 3. The obtained values of the rotational correlation times and anisotropy amplitudes are $\tau_{C2} = 22.5 \pm 0.5$ ns and $r_2 = 0.244 \pm 0.012$, respectively (see Discussion).

Fluorescence Anisotropy Decays of the DnaC−MANT-ATP and DnaC−MANT-ADP Complexes in the Absence of Magnesium. As mentioned above, in the absence of Mg^{2+} cations, the binding of ATP analogue is characterized by a significantly lower affinity as compared to the affinity in the presence of magnesium, while the affinity of ADP analogue is increased (*12*). Moreover, the fluorescence of MANT-ATP in the complex with the DnaC is increased by a factor of ~2, while the fluorescence of bound MANT-ADP is only slightly affected by the absence of magnesium indicating structural difference between the two complexes (*12*).

In the absence of magnesium, the total fluorescence intensity of the MANT-ATP bound to the DnaC is characterized by fluorescence lifetimes $\tau_1 = 9.5 \pm 0.5$ and $\tau_2 = 13.5 \pm 0.5$ ns and relative amplitudes $A_1 = 0.84 \pm 0.01$ and $A_2 = 0.16 \pm 0.01$ (data not shown) (Table 1). The decays of the fluorescence intensities, $I_{VV}(t)$ and $I_{VH}(t)$, of the MANT-ATP bound to the DnaC protein, in the absence of magnesium, are shown in Figure 6a. The difference function, $d(t)$, (eq 2) is shown in Figure 6b. The solid line in Figure 6b is the nonlinear least-squares fit of the experimental curve to eq 2, deconvoluted with the discrete size of the excitation pulse. The single-exponential function provides an adequate description of the decay process. However, unlike in solution containing Mg^{2+}, we observed slight precipitation in solution after the prolong time required to collect both vertical and

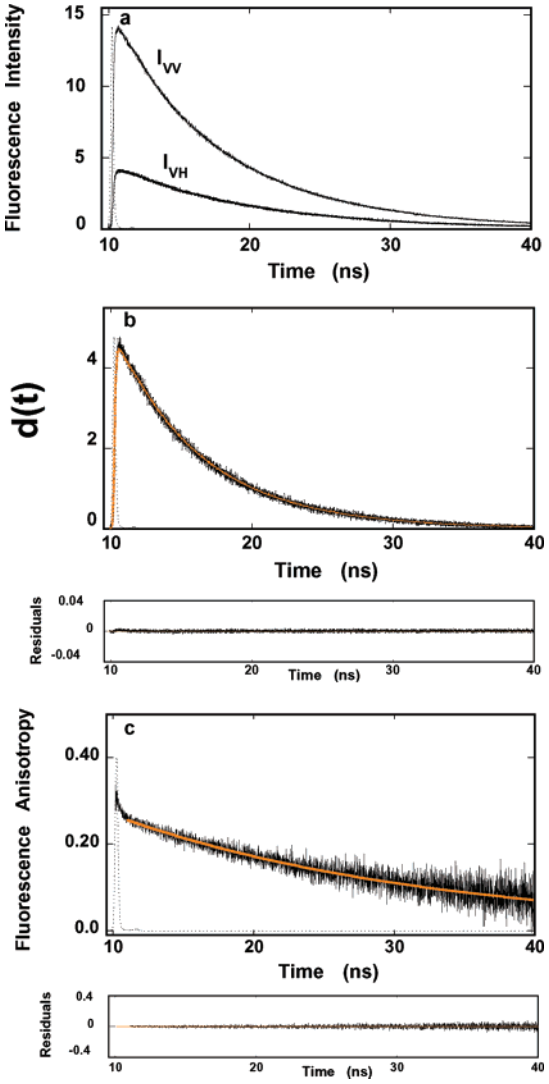

FIGURE 5: (a) Time decays of the MANT-ADP emission in the complex with the DnaC protein (λ_{ex} = 370 nm, λ_{em} = 450 nm) in buffer T4 (pH 8.1, 20 °C), containing 100 mM NaCl and 5 mM $MgCl_2$, with the excitation polarizer oriented vertically and the emission polarizer oriented vertically, $I_{VV}(t)$, and horizontally, $I_{VH}(t)$, respectively. (b) The difference function, $d(t) = I_{VV}(t) - I_{VV}(t)$, as defined by eq 2, obtained from the traces shown in panel a. The solid smooth line is the nonlinear least-squares fit of the experimental curve using one-exponential function defined by eq 2, deconvoluted with the discrete size of the excitation pulse, with rotational correlation time τ_{C2} = 22.8 ns, and corresponding anisotropy amplitude r_2 = 0.267. (c) Time dependence of the MANT-ADP fluorescence anisotropy in the complex with the DnaC protein (λ_{ex} = 370 nm, λ_{em} = 450 nm) in buffer T4 (pH 8.1, 20 °C), containing 100 mM NaCl and 5 mM $MgCl_2$. The solid smooth line is the nonlinear least-squares fit of the experimental curve using eq 3 with a single rotational correlation time τ_{C2} = 22.5 ns, and corresponding anisotropy amplitudes r_2 = 0.244. The dashed lines in all panels are the normalized excitation source profiles. The concentration of the DnaC protein and MANT-ADP are 1.2×10^{-4} M and 5×10^{-6} M, respectively. The zero time is the time corresponding to the center of the excitation pulse.

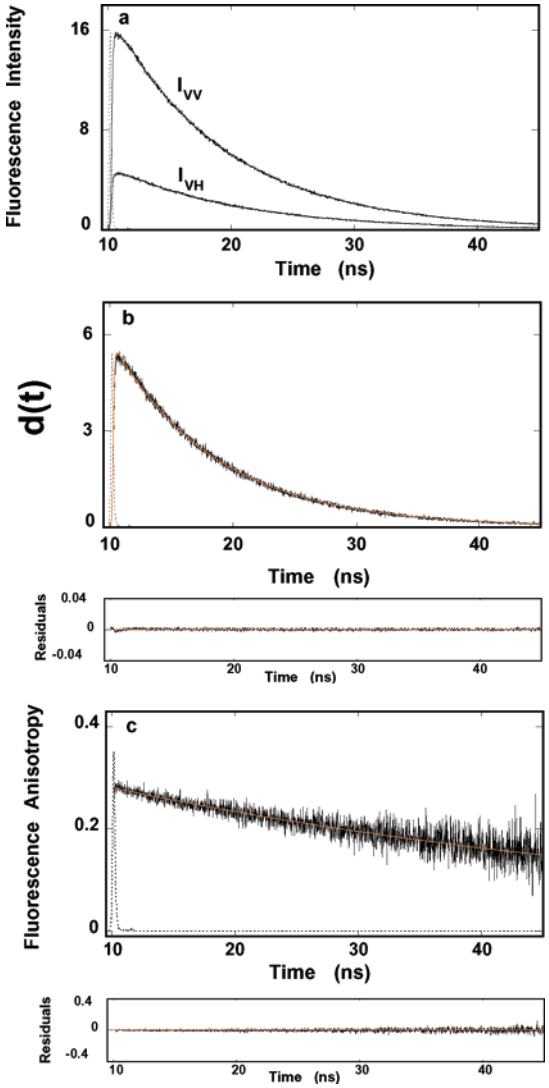

FIGURE 6: (a) Time decays of the MANT-ATP emission in the complex with the DnaC protein (λ_{ex} = 370 nm, λ_{em} = 450 nm) in buffer T4 (pH 8.1, 20 °C), containing 100 mM NaCl, with the excitation polarizer oriented vertically and the emission polarizer oriented vertically, $I_{VV}(t)$, and horizontally, $I_{VH}(t)$, respectively. (b) The difference function, $d(t) = I_{VV}(t) - I_{VV}(t)$, as defined by eq 2, obtained from the traces shown in panel a. The solid smooth line is the nonlinear least-squares fit of the experimental curve using the one-exponential function defined by eq 2, deconvoluted with the discrete size of the excitation pulse, with a single rotational correlation time τ_{C2} = 46.5 ns, and corresponding anisotropy amplitudes r_2 = 0.241. (c). Time dependence of the MANT-ATP fluorescence anisotropy in the complex with the DnaC protein (λ_{ex} = 370 nm, λ_{em} = 450 nm) in buffer T4 (pH 8.1, 20 °C), containing 100 mM NaCl and 5 mM $MgCl_2$. The solid smooth line is the nonlinear least-squares fit of the experimental curve using eq 3 with a single rotational correlation time τ_{C2} = 42.8 ns, and corresponding anisotropy amplitudes r_2 = 0.241. The dashed lines in all panels are the normalized excitation source profiles. The concentration of the DnaC protein and MANT-ATP are 1.2×10^{-4} and 5×10^{-6} M, respectively. The zero time is the time corresponding to the center of the excitation pulse.

horizontal emissions. Different collection times showed no effect on the rotational correlation time however, resulting in a constant, nonzero baseline, b = 0.04 (eq 2). The obtained limiting anisotropy at t = 0, r_{lim}, is only 0.245 ± 0.012, indicating that the observed depolarization process is preceded by another very fast process with the rotational correlation time, τ_{C1}, less than ~50 ps (see above). The resolved rotational correlation time of the complex is τ_{C2} = 46.5 ± 3 ns, much longer than observed in the presence of magnesium (Table 1). The direct time dependence of the fluorescence anisotropy of MANT-ATP−DnaC complex in buffer T4 (pH 8.1, 20 °C), containing 100 mM NaCl, is shown in Figure 6c. The initial unresolved part of the plot is affected by the discrete size of the excitation pulse;

nevertheless, the data indicate that, in the complex, a very fast fluorescence depolarization of the MANT-ATP fluorescence occurs within the time range shorter than one nanosecond (see above). The solid line in Figure 6c is a nonlinear least-squares fit of the experimental curve, in the range above 2 ns, using single-exponential function defined by eq 3. The theoretical line provides an adequate fit for experimental curve with the baseline $b = 0.048$. The obtained values of the rotational correlation times and anisotropy amplitude of the decay process are $\tau_{C2} = 42.8 \pm 2.1$ ns and $r_2 = 0.241 \pm 0.02$, respectively, in good agreement with the deconvolution result of the difference function d(t) (Figure 6b).

A different behavior is observed in the case of the MANT-ADP−DnaC complex in the absence of magnesium (data not shown). The total fluorescence intensity of the MANT-ADP bound to the DnaC is characterized by fluorescence lifetimes $\tau_1 = 6.8 \pm 0.3$ and $\tau_2 = 9.9 \pm 0.5$ ns and relative amplitudes $A_1 = 0.18 \pm 0.01$ and $A_2 = 0.82 \pm 0.01$ (Table 1). These values are similar to the same parameters observed in the presence of magnesium. The difference function, d(t), and the direct anisotropy decay are described by the single-exponential function. Unlike the MANT-ATP−DnaC complex, we did not detect any precipitation of the MANT-ADP−DnaC complex in the absence of magnesium, resulting in the baseline value $b = 0$. The limiting anisotropy $r_{lim} = 0.303 \pm 0.015$ and is higher than observed in the absence of Mg^{2+}. The resolved rotational correlation time of the complex is $\tau_{C2} = 22.3 \pm 0.5$ ns, is, within the experimental accuracy, the same as obtained for the MANT-ADP−DnaC complex in the presence of magnesium. However, it is much shorter than observed for the analogous MANT-ATP−DnaC complex (Table 1).

DISCUSSION

The Replication Factor DnaC Protein Is a Monomer in Examined Solution Conditions in the Presence of Magnesium, ATP, and ADP. The independence of the sedimentation coefficient, $s_{20,w}$, of the DnaC protein upon the protein concentration shows that, in solution, the replication factor exclusively exists as a monomer (Figures 1 and 2) (*42*, *43*). Thermodynamic, spectroscopic, and kinetic studies showed that binding of magnesium, ATP, and ADP induce specific conformational changes in the DnaC protein molecule (*12*−*14*) (see above). The results obtained in this work indicate that structural changes induced by binding of magnesium and/or nucleotide cofactors do not lead to the DnaC protein association. The fact that the protein is exclusively in a monomeric state in the presence of both, ATP or ADP, has important functional implications. Recall, current views are that the biological function of the DnaC protein is strictly related to its interactions with the *E. coli* primary replicative helicase the DnaB protein (*1*−*7*). Our recent quantitative studies of the DnaC binding to the DnaB hexamer show that six molecules of the replication factor bind with positive cooperativity to the helicase hexamer (*15*). The lack of any oligomerization process in the presence of Mg^{2+}, ATP, and/or ADP indicates that the positive cooperative interactions among bound DnaC molecules are not an intrinsic property of the DnaC protein. Rather, it indicates that the cooperative interactions observed in the DnaC−DnaB complex are exclusively induced by interactions with the helicase. Notice the fact that the binding of the DnaC protein to the helicase is independent, whether the magnesium-binding site(s) or nucleotide-binding site of the protein is saturated with nucleotide cofactor, corroborates very well with this conclusion (*15*).

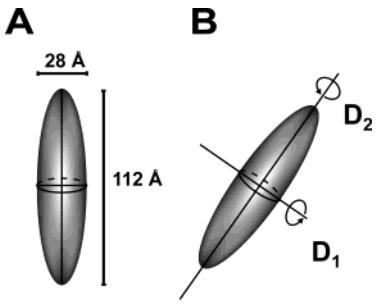

FIGURE 7: (A) Model of the DnaC protein represented as prolate ellipsoid of revolution, based on the hydrodynamic results obtained in this work. The long axis of the molecule is $a = 112$ Å and the short axis $b = 28$ Å. (B) Two rotational movements of the molecule represented by a prolate ellipsoid (arrows), around the short and long axis of the molecule, described by the rotational diffusion coefficients, D_1 and D_2, that define the rotational correlation times (see text for details).

DnaC Protein in Solution Has an Elongated Structure with the Axial Ratio of 4:1 When Modeled as a Prolate Ellipsoid, Little Affected by the Binding of the Nucleotide Cofactors. The sedimentation velocity studies provide the first information about the shape of the DnaC molecule in solution. Using the estimated degree of hydration of the protein, $h = 0.273$ $g_{H_2O}/g_{protein}$, the value of $s^{\circ}_{20,w} = 2.45 \pm 0.07$ indicates that, when modeled as prolate ellipsoid of revolution, the molecule has axial ratio of $p = 4.0 \pm 0.6$ (*31*−*33*). Thus, sedimentation velocity data clearly indicate that the DnaC molecule is not spherical, but it has a considerably elongated structure. Even with the estimated maximum degree of hydration, $h = 0.39$ $g_{H_2O}/g_{protein}$, the axial ratio, $p = 3.4 \pm 0.5$. This value is within the determined range of p and indicates an elongated shape of the molecule. Using $p = 4$ together with the model-independent hydrated volume of the molecule, $V_h = M(\bar{\nu} + h\bar{\nu}_S)N_A$, and the expression for the volume of the prolate ellipsoid $V = 4\pi ab^2$, one obtained dimensions of the axes of the hydrated protein molecule as $2a = 112$ Å and $2b = 28$ Å, as depicted in Figure 7A.

The same values of the sedimentation coefficient in the presence of magnesium, ATP, or ADP indicate that binding of Mg^{2+} cations and nucleotide cofactors does not significantly affect the global conformation of the DnaC protein as sensed by sedimentation velocity. i.e., the translational movement (Figure 1) (*31*−*33*). As mentioned above, these results may be surprising in the light of binding and kinetic studies indicating that both magnesium and nucleotide cofactors affect the protein conformation (*12*−*14*). However, the hydrodynamic data indicate that the observed conformational changes must predominantly have a local character (see below). Notice, in the complex with the DnaB helicase, the DnaC protein binds to the 33-kDa large domain of the enzyme, at a significant distance from the small 12-kDa domain (*15*, *44*). It is interesting to compare the estimated dimensions of the DnaC molecule with the size of the large domain of the DnaB helicase. Electron microscopy studies indicate that part of the large domain, separated from the small 12-kDa domain, extends over a distance of 60−80 Å

(*44*−*46*). Moreover, this part of the large domain is easily accessible to the solvent (*46*). Such a large and accessible structural element of the helicase provides enough surface area to accommodate the elongated DnaC molecule in the way that is consistent with the hydrodynamic properties of the DnaC−DnaB complex (*15*).

In general, the fluorescence anisotropy decay of a macromolecule, modeled as a prolate ellipsoid of revolution, is described by a three-exponential function (*25*, *47*−*49*). Thus, the presence of only a single rotational correlation time in the time region corresponding to the rotation of the entire DnaC−nucleotide cofactor complex, would suggest that the protein has a spherical structure, contrary to the results obtained from sedimentation velocity analysis discussed above (Figures 4 and 5). However, for the spherical protein with the hydrated volume corresponding to the DnaC protein, the expected rotational correlation time in the examined solution conditions, is $\tau_C = 14.9$ ns, while, in the presence of magnesium, the experimentally observed values of τ_{C2} are 21.7 ± 0.5 and 22.8 ± 0.5 ns for the complexes with ATP or ADP, respectively (Figures 4 and 5, Table 1). The large difference between the expected and measured τ_C clearly indicates a significantly nonspherical structure of the protein molecule (*47*−*49*). Therefore, the presence of only a single rotational correlation time must result from specific characteristics of the DnaC−nucleotide cofactor system. We examine the most plausible scenarios below.

The excitation anisotropy spectra of the MANT-ATP and MANT-ADP complexes with the DnaC protein indicate that the maximum value of the anisotropy is reached at the excitation wavelength above 360 nm (Galletto et al., to be published). Because the excitation wavelength in our experiments is at 370 nm, far in the red side of the absorption spectrum, the absorption and emission dipoles can be treated as parallel (*47*−*49*). Separation of two depolarization processes by at least a factor of an ∼400 on the time scale of the experiment indicates that they are effectively decoupled. In such case, if the emission dipole is at a fixed angle Θ with respect to the major axis of the ellipsoid the part of the observed anisotropy decay of the protein−nucleotide complex, modeled as a prolate ellipsoid of revolution, is described by a three-exponential function (*47*−*50*).

$$r(t) = r_{lim}\left\{\left[\frac{3}{4}\sin^2 2\Theta\right]\exp\left(-\frac{t}{\tau_{CP1}}\right) + \frac{3}{4}[\sin^4\Theta]\exp\left(-\frac{t}{\tau_{CP2}}\right) + \frac{1}{4}[(3\cos^2\Theta - 1)^2]\exp\left(-\frac{t}{\tau_{CP3}}\right)\right\} \quad (7)$$

The value of the limiting anisotropy, r_{lim}, corresponds to the observed anisotropy amplitude of the slow depolarization process. In the case of the DnaC−MANT-ATP complex, $r_{lim} \approx 0.241-0.252$ (see above). The three rotational correlation times are defined as

$$\tau_{CP1} = \frac{1}{D_1 + 5D_2} \quad \tau_{CP2} = \frac{1}{4D_1 + 2D_2} \quad \tau_{CP3} = \frac{1}{6D_2} \quad (8)$$

where D_1 and D_2 are the rotational diffusion coefficients of the ellipsoid along its major and short axes, respectively (Figure 7B) (*47*−*49*). The rotational diffusion coefficients are related to the axial ratio of the ellipsoid, *p*, and the hydrated volume of the corresponding sphere by the expressions

$$D_1 = \left[\frac{3p(p-Q)}{2(p^2-1)}\right]\frac{kT}{6\eta M(\bar{v} + h\bar{\nu}_S)}$$

$$D_2 = \left[\frac{3p(2p^2-1)Q - p}{2(p^4-1)}\right]\frac{kT}{6\eta M(\bar{\nu} + h\bar{\nu}_S)} \quad (9a)$$

where

$$Q = \frac{\ln[p + \sqrt{p^2-1}]}{\sqrt{p^2-1}} \quad (9b)$$

Thus, for a given $\bar{\nu}$ and *h*, the rotational correlation times of the anisotropy decay depend only on the axial ratio of the ellipsoid, *p*, while the amplitudes are exclusively the functions of the angle, Θ.

In the examined solution conditions (buffer T4), the rotational correlation times for the protein with the axial ratio $p = 4$, as described by eqs 8−9, are $\tau_{CP1} = 31.3$, $\tau_{CP2} = 14.6$, and $\tau_{CP3} = 50.9$ ns. Figure 8a shows computer simulations of the anisotropy decay, using eq 7, for three different values of the angle Θ, 90°, 45 °, and 0° from the possible range of the Θ values i.e., from 0° to 90°. For these simulations, the value of r_{lim} has been taken as 0.241. For comparison, the decay of the anisotropy with a single rotational correlation time $\tau_C = 21.7$ ns as experimentally observed is also included. The value of $\Theta = 90°$ gives a curve that decays in a shorter time range than the experimental obtained correlation time. It is dominated by $\tau_{CP2} = 14.6$ ns, with some contribution from the decay mode characterized by $\tau_{C3} = 50.9$ ns, i.e., it cannot be described by a single-exponential function. On the other hand, the curves with $\Theta = 45°$ and $\Theta = 0°$ decay in the time range significantly longer than observed for the DnaC−MANT-ATP complex. For $\Theta = 0°$, amplitudes associated with τ_{CP1} and τ_{CP2} are zero (eq 7) and the overall decay is a single-exponential function characterized by the $\tau_{CP3} = 50.9$ ns. This value is much longer than the experimentally observed correlation time of 21.7 ns. In fact, there is not a fixed value of Θ that, when introduced to eq 7, would provide a decay curve indistinguishable from the curve with an experimentally observed single rotational correlation time of 21.7 ns.

With a fixed value of Θ, another possibility is that the observed single rotational correlation time in the experimental anisotropy decay is an average of the three correlation times in eq 7, τ_{Cav}, weighted by the appropriate values of three amplitudes. The anisotropy decay is then described by a single-exponential function

$$r(t) = r_{lim}\left[\exp\left(-\frac{t}{\tau_{Cav}}\right)\right] \quad (10a)$$

and the average rotational correlation time, τ_{Cav}, is

$$\tau_{Cav} = \frac{\int_0^\infty r(t)dt}{r_o} = \left[\frac{3}{4}\sin^2 2\Theta\right]\tau_{C1} + \frac{3}{4}[\sin^4\Theta]\tau_{C2} + \frac{1}{4}[(3\cos^2\Theta - 1)^2]\tau_{C3} \quad (10b)$$

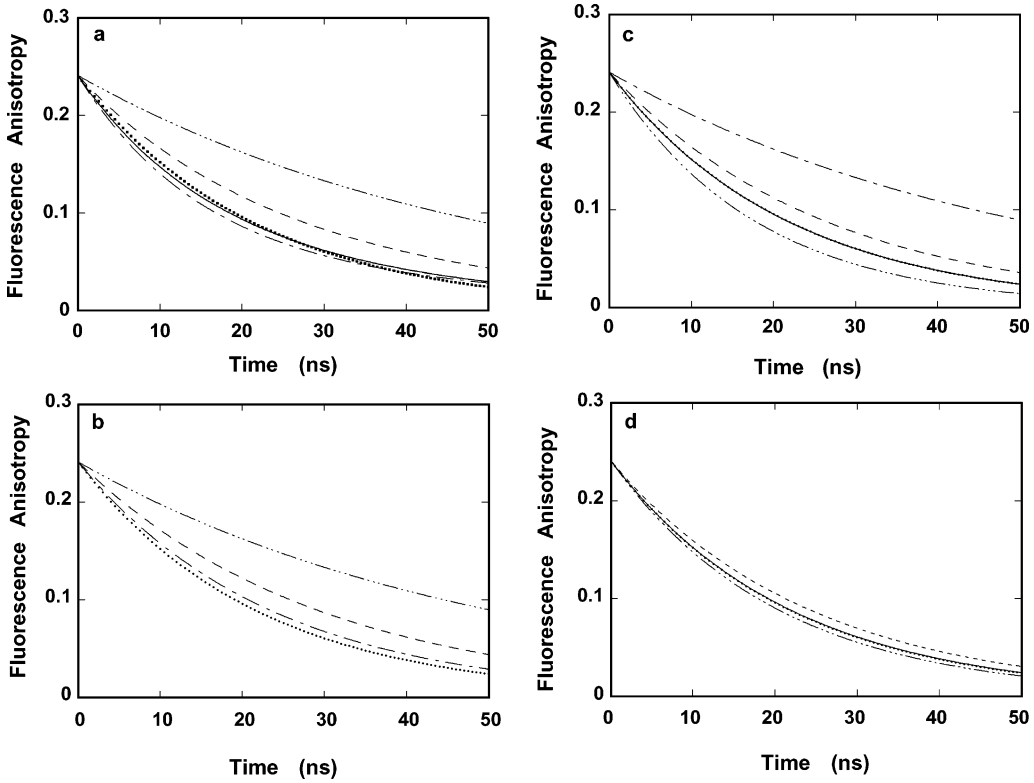

FIGURE 8: (a) Computer simulations of the fluorescence anisotropy decay, $r(t)$, of the prolate ellipsoid of revolution (Figure 7), as defined by eq 7, for three different values of the angle Θ between the emission dipole and the major axis of the ellipsoid, a; (− - −) 90°, (− − −) 45°, (− - - - −) 0°. The dotted line (**...**) is the fluorescence anisotropy decay with the single rotational correlation time, $\tau_C = 21.7$ ns, corresponding to the DnaC protein−MANT-ATP complex. The solid line (—) is the computer best fit of the fluorescence anisotropy decay, with experimentally obtained single rotational correlation time $\tau_C = 21.7$ ns, with Θ = 68°. (b) Computer simulations of the fluorescence anisotropy decay, $r(t)$, of the prolate ellipsoid of revolution, using a single, average rotational correlation time, τ_{Cav}, as defined by eqs 10a and 10b, for three different values of the angle Θ between the emission dipole and the major axis of the ellipsoid, a; (− - −) 90°, (− − −) 45°, (− - - - −) 0°. The dotted line (**...**) is the fluorescence anisotropy decay with the single rotational correlation time, $\tau_C = 21.7$ ns, corresponding to the DnaC protein−MANT-ATP complex. (c) Computer simulations of the fluorescence anisotropy decay, $r(t)$, of the prolate ellipsoid of revolution, using a single, harmonic average rotational correlation time, τ_{CH}, as defined by eq 11a and 11b, for three different values of the angle Θ between the emission dipole and the major axis of the ellipsoid, a; (− - −) 90°, (− − −) 45°, (− - - - −) 0°. The dotted line (**...**) is the fluorescence anisotropy decay with the single rotational correlation time, $\tau_C = 21.7$ ns, corresponding to the DnaC protein−MANT-ATP complex. The solid line (—) is the computer best fit of the fluorescence anisotropy decay, with experimentally obtained single rotational correlation time $\tau_C = 21.7$ ns, with Θ = 58°. (d) Computer simulations of the fluorescence anisotropy decay, $r(t)$, for the prolate ellipsoid of revolution, using a single, harmonic average rotational correlation time, τ_{CH}, for the random orientation of the emission dipole with respect to the major axis of the ellipsoid, as defined by eqs 12a and 12b, for three different values of the ellipsoid axial ratio, p; (− - −) $p = 3$, (− − −) $p = 3.6$, (− - - - −) $p = 5$ (see text for details). The dotted line (**...**) is the fluorescence anisotropy decay with the single rotational correlation time, $\tau_C = 21.7$ ns, corresponding to the experimental value obtained for the DnaC protein−MANT-ATP complex. In all panels, the selected $r_{lim} = 0.241$.

where $r(t)$ in eq 10b is defined by eq 7. Figure 8b shows the computer simulations of the anisotropy decay, using eqs 10a and 10b, for three different values of Θ, 90°, 45°, and 0° together with the decay of the anisotropy with a single rotational correlation time $\tau_C = 21.7$ ns. Even with Θ = 90° the decay is characterized by τ_{Cav} larger than experimentally observed. In fact, for most of Θ values the average rotational correlation time of the macromolecule with $p = 4$ and molecular weight corresponding to the DnaC protein, the average rotational correlation time is in the range of ∼30 ns (Figure 8b). Thus, similar to the general fixed angle case considered above, there is not a fixed value of Θ, which would provide a decay curve with a single average rotational correlation time, τ_{Cav}, as defined by eq 10a, that is superimposable on the experimentally observed decay with $\tau_C = 21.7$ ns.

Notice that the analyses discussed so far (Figure 8a,b) assume that the fluorescence lifetime of the fluorophore is very similar to the rotational correlation time of the protein−nucleotide complex. However, in the case of the DnaC−MANT-ATP−Mg^{2+} complex only ∼80% of the fluorescence intensity decay is characterized by a fluorescence lifetime $\tau \sim 9$ ns, which is still by a factor of ∼2 shorter than predicted τ_{Cav} for the DnaC protein with $p = 4$ (see above). Such property of the system suggests that the observed anisotropy decay may be approximated by a single rotational correlation time, τ_{CH}, that is a harmonic average of the three correlation times in eq 7, as (*48*)

$$r(t) = r_{lim}\left[\exp\left(-\frac{t}{\tau_{CH}}\right)\right] \tag{11a}$$

and

$$\tau_{CH} = \frac{\frac{3}{4}(\sin^2 2\Theta)}{\tau_{C1}} + \frac{\frac{3}{4}(\sin^4 \Theta)}{\tau_{C2}} + \frac{\frac{1}{4}[(3\cos^2 \Theta - 1)^2]}{\tau_{C3}} \tag{11b}$$

The computer simulations of the anisotropy decay for a

prolate ellipsoid corresponding to the DnaC−MANT-ATP−Mg^{2+} complex with an axial ratio $p = 4$, using harmonic average rotational correlation time defined by eqs 11a and 11b, for Θ equal 90°, 45°, and 0° are shown in Figure 8c. The decay of the anisotropy with the experimentally observed, single rotational correlation time $\tau_C = 21.7$ ns falls between $\Theta = 90°$ and 45°, respectively. However, when $\Theta = 58°$, the theoretical decay (dashed line) is virtually indistinguishable from the curve described by $\tau_C = 21.7$ ns. Thus, the approximation of the experimental decay of the DnaC−MANT-ATP−Mg^{2+} complex using the harmonic average of the rotational correlation time provides an excellent description of the experimental data for the prolate ellipsoid, corresponding to the macromolecule with the axial ratio $p = 4$ and the fixed angle between the emission dipole and the major axis of the ellipsoid $\Theta = 58°$.

The analyses above use the axial ratio of the DnaC protein molecule determined from the sedimentation velocity studies (see above). The fact that harmonic average rotational correlation time is the most plausible in describing the experimentally obtained fluorescence anisotropy decay of the DnaC−MANT-ATP−Mg^{2+} complex allows us to utilize another characteristic behavior of the DnaC−nucleotide complex to obtain the approximate value of the axial ratio, *p*, independently from the sedimentation velocity data. Recall, the fast depolarization process in the experimental anisotropy decay is ∼400 faster than the slow depolarization resulting from the rotation of the entire complex. The fast process reduces the initial anisotropy and may introduce randomization of the location of the emission dipole with respect to the major axis of the ellipsoid. In other words, one can assume that the bound nucleotide undergoes a fast isotropic rotation before the protein rotation affects the depolarization to any detectable degree. As a result, the sample would contain a population of protein−nucleotide cofactor complexes with emission dipoles randomly oriented with respect to the major axis of the ellipsoid and not located at a fixed angle Θ. In such case, the fluorescence anisotropy decay of the prolate ellipsoid is described by an expression (*47*, *48*)

$$r(t) = r_o\left[0.4\exp\left(-\frac{t}{\tau_{CP1}}\right) + 0.4\exp\left(-\frac{t}{\tau_{CP2}}\right) + 0.2\exp\left(-\frac{t}{\tau_{CP3}}\right)\right] \quad (12a)$$

The harmonic average correlation time, τ_{CH}, is then defined as

$$\tau_{CH} = \frac{0.4}{\tau_{CP1}} + \frac{0.4}{\tau_{CP2}} + \frac{0.2}{\tau_{CP3}} \quad (12b)$$

Notice, with the assumption of random orientation of the emission dipole, both anisotropy decay and the harmonic average rotational correlation time are independent of Θ. They are sole functions of the axial ratio, *p*, of the ellipsoid.

Figure 8d shows computer simulations of fluorescence anisotropy decays, using eqs 12a−12b for a prolate ellipsoid corresponding to the DnaC−MANT-ATP−Mg^{2+} complex, for different values of the axial ratio, *p*. The anisotropy decay for a single correlation time $\tau_C = 21.7$ ns, corresponding to the experimentally determined value, is also included. It is evident that the ellipsoid model with an axial ratio neither $p = 3$ nor $p = 5$ represents the experimentally obtained decay. However, the ellipsoid model with the axial ratio $p = 3.6$ is indistinguishable from the experimental data. This value of *p* is in good agreement with the axial ratio of $p = 4 \pm 0.6$ determined in independent sedimentation studies (see above). Nevertheless, the smaller value of the axial ratio suggests that either the nucleotide binding site experiences some segmental motion with respect the rest of the DnaC molecule on the nanosecond time scale to the extent that is not sensed by the translational motion examined in the sedimentation velocity studies, or the protein assumes a slightly less elongated shape, when associated with ATP.

Analogous analyses have been performed for the DnaC−MANT-ADP complex. The experimentally determined single rotational correlation time, $\tau_C = 22.8 \pm 0.5$ ns is slightly longer than observed in the presence of the ATP analogue. Neither a general nor the average correlation time model with a fixed Θ angle (eqs 7 and 10a−10b) provides the decay curve superimposable on the experimentally obtained decay with $\tau_C = 22.8$ ns (data not shown). However, when using the harmonic average rotational correlation time and the assumption of random orientation of the emission dipole (eqs 12a−12b), the value of $\tau_C = 22.8 \pm 0.5$ ns corresponds to the prolate ellipsoid of revolution with the axial ratio $p = 4.1$. This value of the axial ratio is in excellent agreement within the sedimentation velocity results. Nevertheless, the longer rotational correlation time, and larger corresponding axial ratio, as compared to the complex with the ATP analogue, suggest that in the complex with the ADP analogue the DnaC protein has slightly more elongated global structure than in the complex with ATP.

Allosteric Interactions Between Magnesium and Nucleotide-Binding Site Affect Dramatically the Dynamics of the Bound ATP Analogue. Equilibrium studies provided the first indication of strong allosteric interactions between the magnesium and the nucleotide-binding site of the DnaC protein as reflected by striking differences between the ATP and ADP analogue binding in the absence of Mg^{2+} (*12*). The ATP affinity is diminished by a factor of ∼6 and the fluorescence intensity, at saturation, is increased by a factor of ∼2, while ADP affinity is increased 2-fold and the fluorescence of the complex is similar to the one observed in the presence of magnesium. Saturation of the magnesium effect occurs at $[Mg^{2+}] \sim 10^{-4}$ M, indicating that the involved magnesium-binding sites have affinity characterized by the binding constant $>10^5$ M^{-1} (*12*). Such a large value of the binding constant effectively excludes the possibility that the binding of Mg^{2+} to the nucleotide is predominantly responsible for the observed effect in the examined solution conditions (100 mM NaCl) (*12*).

Sedimentation velocity data indicate that, in the absence of Mg^{2+}, both ATP and ADP complexes with the DnaC protein have the same sedimentation coefficients as observed in the presence of magnesium, i.e., their global structures are unaffected by the magnesium cation binding (Figure 1b,c). Yet, their rotational correlation times, τ_{C2}, are remarkably different. While the complex with the ADP analogue is characterized by the value of $\tau_{C2} = 22.3 \pm 0.5$ ns, the same, within experimental accuracy, as observed in the presence of Mg^{2+}, the complex with the MANT-ATP has $\tau_{C2} = 46.5 \pm 3$ ns as compared to 21.7 ± 0.5 ns in the presence of magnesium (Figure 6c, Table 1).

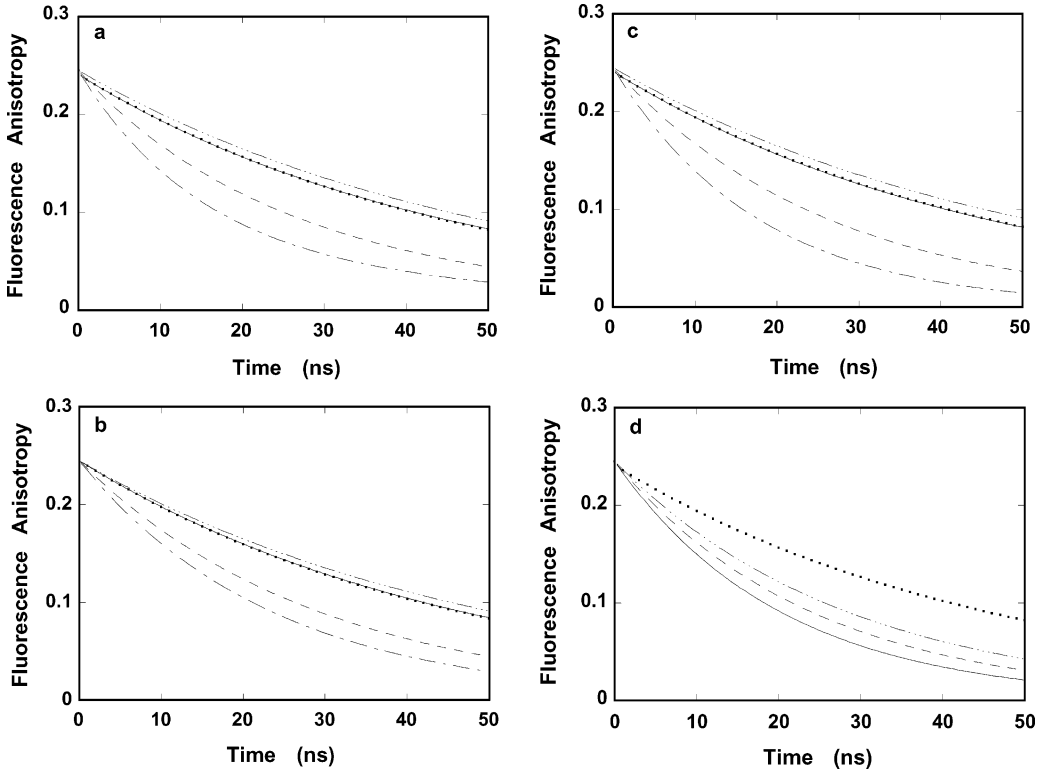

FIGURE 9: (a) Computer simulations of the fluorescence anisotropy decay, $r(t)$, of the prolate ellipsoid of revolution (Figure 7), as defined by eq 7, for different values of the angle Θ between the emission dipole and the major axis of the ellipsoid, a; (− - −) 90°, (− − −) 45°, (− - - - −) 0°. The value of $r(0) = 0.245$ is taken as experimentally obtained for the DnaC protein−MANTATP complex in buffer T4 (pH 8.1, 20 °C), containing 100 mM NaCl (Table 2). The dotted line (**...**) is the fluorescence anisotropy decay with the single rotational correlation time, $\tau_C = 46.5$ ns, corresponding to the DnaC protein−MANT-ATP complex. The solid line (—) is the computer simulation of the fluorescence anisotropy decay, with experimentally obtained single rotational correlation time $\tau_C = 46.5$ ns, with $\Theta = 13.5°$. (b) Computer simulations of the fluorescence anisotropy decay, $r(t)$, of the prolate ellipsoid of revolution, using a single, average rotational correlation time, τ_{Cav}, as defined by eqs 10a and 10b, for different values of the angle Θ between the emission dipole and the major axis of the ellipsoid, a; (− - −) 90°, (− − −) 45°, (− - - - −) 0°. The dotted line (**...**) is the fluorescence anisotropy decay with the single rotational correlation time, $\tau_C = 46.5$ ns, corresponding to the DnaC protein−MANT-ATP complex. The solid line (—) is the computer simulation of the fluorescence anisotropy decay, with experimentally obtained single rotational correlation time $\tau_C = 46.5$ ns, with $\Theta = 15°$. (c) Computer simulations of the fluorescence anisotropy decay, $r(t)$, of the prolate ellipsoid of revolution, using a single, harmonic average rotational correlation time, τCH, as defined by eqs 11a and 11b, for different values of the angle Θ between the emission dipole and the major axis of the ellipsoid, a; (− - −) 90°, (− − −) 45 °, (− - - - −) 0°. The dotted line (**...**) is the fluorescence anisotropy decay with the single rotational correlation time, $\tau_C = 46.5$ ns, corresponding to the DnaC protein−MANT-ATP complex. The solid line (—) is the computer best fit of the fluorescence anisotropy decay, with experimentally obtained single rotational correlation time $\tau_C = 46.5$ ns, with $\Theta = 13°$. (d) Computer simulations of the fluorescence anisotropy decay, $r(t)$, for the prolate ellipsoid of revolution, using a single, harmonic average rotational correlation time, τ_{CH}, for the random orientation of the emission dipole with respect to the major axis of the ellipsoid, as defined by eqs 12a and 12b, for three different values of the ellipsoid axial ratio, p; (____) $p = 3$, (__ __ __) $p = 5$, (____ _ _ ___) $p = 15$ (see text for details). The dotted line (**...**) is the fluorescence anisotropy decay with the single rotational correlation time, $\tau_C = 46.5$ ns, corresponding to the experimental value obtained for the DnaC protein−MANT-ATP complex. In all panels, the value of $r_{lim} = 0.245$.

Figure 9a shows computer simulations of the anisotropy decay, for a prolate ellipsoid corresponding to the DnaC−MANT-ATP−complex with an axial ratio $p = 4$, using eq 7, for four different values of the angle Θ, 90°, 45°, 13.5°, 0°. The decay of the anisotropy with a single rotational correlation time $\tau_C = 46.5$ ns, as experimentally observed, is also included. Only the curves with $\Theta = 0°$ decays with rotational correlation time, longer (50.9 ns) than observed for the DnaC−MANT-ATP complex in the absence of magnesium. However, with a fixed value of $\Theta = 13.5°$ the theoretical line is indistinguishable from the curve with the experimentally observed rotational correlation time. Figure 9b shows the computer simulations of the anisotropy decay for the average rotational correlation time, τ_{Cav}, as described by eqs 10a and 10b, for four different values of Θ, 90°, 45°, 15°, and 0° together with the decay of the anisotropy with a single rotational correlation time $\tau_C = 46.5$ ns. Thus, similar to the general fixed angle case (Figure 9a), a fixed value of $\Theta = 15°$ provides a decay curve with a single average rotational correlation time, τ_{Cav}, that is superimposable on the experimentally observed decay with $\tau_C = 46.5$ ns. The final fixed angle case is an approximation of the anisotropy decay by a single harmonic average correlation time, τ_{CH}, as defined by eqs 11. The computer simulations of the anisotropy decay using harmonic average rotational correlation time for Θ equal 90°, 45°, 13°, and 0° are shown in Figure 9c. The decay of the anisotropy with the experimentally observed, single rotational correlation time $\tau_C = 46.5$ ns is superimposable on the theoretical line with $\Theta = 13°$. Thus, the experimental anisotropy decay of the DnaC−MANT-ATP complex in the absence of magnesium can be described by all three cases using the fixed angle between the emission dipole of the MANT chromophore and the long axis of the ellipsoid, $\Theta = 13-15°$.

However, a very different behavior is observed if the random orientation of the emission dipole is assumed as

suggested by low value of the limiting anisotropy $r_{lim} = 0.245 \pm 0.012$ (Table 1) (see above). Figure 9d shows computer simulations of fluorescence anisotropy decays, using eqs 12a−12b for a prolate ellipsoid corresponding to the DnaC−MANT-ATP complex, for different values of the axial ratio, *p*, together with the anisotropy decay for a single correlation time $\tau_C = 46.5$ ns, corresponding to the experimentally determined value. As indicated by the plots, even with $p = 15$, the theoretical decay curve does represent the experimentally obtained rotational correlation time. In fact, there is not a physically realistic value of *p* that could represent the experimentally observed harmonic average rotational correlation time with the assumption of the random orientation of the emission dipole (Figure 9d).

It is evident that the assumption of random orientation of the emission dipole does not apply to the MANT-ATP−DnaC complex in the absence of magnesium. The computer simulations strongly suggest that the nature of the fast anisotropy decay process, that results in the limiting anisotropy $r_{lim} = 0.245 \pm 0.012$, is different in the absence of Mg^{2+} (Table 1). The fact that fixed angle models can represent the experimental decay strongly suggests that the fast decay is not a random isotropic rotation of the bound nucleotide, as observed in the presence of magnesium, but rather a fast reorientation to a specific location. This specific location is characterized by a fixed angle between the emission dipole and the major axis of the ellipsoid, $\Theta \approx 13-16°$ (Figure 9). In other words, in the absence of magnesium, the observed rotation of MANT-ATP−DnaC complex occurs close to around the long axis of the ellipsoid, resulting in the long rotational correlation time of the DnaC−nucleotide complex, without any change in the global conformation of the complex, as indicated by the unaffected sedimentation coefficient (Figure 1c).

Results of the combined application of the sedimentation velocity and fluorescence anisotropy methods, reported in this work, have a significant importance for our understanding of the DnaC protein structure and the structure of its complexes with the nucleotide cofactors. Both methods indicate that the protein has an elongated shape with the axial ratio $p \sim 4$ when modeled as prolate ellipsoid of revolution. Recall, the DnaC protein exists in equilibrium between two structural states prior to the nucleotide binding (*12*−*14*). The nucleotide cofactors bind exclusively to one conformation, i.e., at saturation, the protein−nucleotide cofactor complex is exclusively in one conformational state (*12*−*14*). Similar axial ratios observed for the free protein and the complexes with nucleotide cofactors indicate that the two conformations of the DnaC protein prior to the ATP or ADP binding have similar global structure, suggesting that the difference between the two conformations is limited to the protein's surface. Thus, the data strongly suggest that the protein has a rigid global structure on the nanosecond time scale, not affected by the nucleotide cofactors. Nevertheless, there are differences between the complexes with ATP and ADP. The anisotropy data indicate that, in the presence of Mg^{2+}, a complex with ATP has a more flexible structure around the nucleotide-binding site, while the complex with ADP seems to be more rigid with the protein assuming also a slightly more elongated global shape. Magnesium exerts control predominantly on the complex with the ATP analogue. In the absence of magnesium, the ATP analogue is firmly held in the binding site. In the presence of Mg^{2+}, this fixed location is released. The bound ATP analogue is allowed to assume a flexible conformational state. Such transition from a fixed location to a flexible complex may play an important role in fast responses of the DnaC protein conformation, with bound ATP, to the changing environment in the replication fork machinery.

Notice the energetics of the binding of the DnaC protein to the large domain of the DnaB helicase is indistinguishable in the presence of ATP or ADP analogues (*12*). However, the structures of both complexes differ with the DnaC protein located at a further distance from the small domain of the helicase in the presence of ADP. Such behavior would occur if the DnaC protein has a more elongated shape in the presence of ADP, as suggested by the anisotropy data (see above). The fact that the nucleotide analogues can bind with unchanged affinity to the DnaC protein bound to the DnaB helicase indicates that the DnaC nucleotide-binding site is located on the outside surface of the protein, i.e., not engaged in interactions with the DnaB helicase (*12*). These data indicate that the surface interacting with the helicase is not affected by the cofactors. On the other hand, the outside surface that is exposed to interactions with the remaining ingredients of the replication fork, responds differently to ATP than to ADP in a process controlled by magnesium. Altogether, the obtained results strongly suggest that the DnaC protein is a rigid link between the DnaB helicase and the remaining parts of the replication fork apparatus. If the nucleotide binding to the DnaC protein controls the DnaC−helicase complex interactions within the replication fork machine then the obtained data indicate that it predominantly occurs through the conformational changes of the DnaC protein surface, differently induced by ATP and ADP, rather than the global conformational changes of the entire protein. Our laboratory is currently examining this possibility.

ACKNOWLEDGMENT

We wish to thank Mrs. Betty Sordahl for reading the manuscript.

REFERENCES

1. Kornberg, A., and Baker, T. A. (1992) *DNA Replication*, pp 275−306, Freeman, San Francis.
2. Marians, K. J. (1992) Prokaryotic DNA replication, *Annu. Rev. Biochem. 61*, 673−719.
3. Marians, K. J. (1999) PriA: at the crossroads of DNA replication and recombination, *Prog. Nucl. Acid. Res., Mol. Biol. 63*, 39−67.
4. Wickner, S., and Hurwitz, J. (1973) Interactions of *Escherichia coli* dnaB and dnaC (D) Gene Products In Vitro, *Proc. Natl. Acad. Sci. U.S.A. 72*, 783−787.
5. (a) Skarstad, K., and Wold, S. (1995) The Speed of the *Escherichia coli* fork in vivo depends on the DnaB-DnaC ratio, *Mol. Microbiol. 17*, 825−831. (b) Wechsler, J. (1975) Genetic and phenotypic characterization of dnaC mutations, *J. Bacteriol. 121*, 594−599.
6. Wechsler, J., and Gross, J. D. (1971) *Escherichia coli* mutants temperature-sensitive for DNA synthesis, *Mol. Gen. Genet. 113*, 273−284.
7. Sancar, A., and Hearst, J. E. (1993) Molecular matchmakers, *Science 259*, 1415−1420.
8. Marszalek, J., and Kaguni, J. M. (2001) DnaA protein directs the binding of the DnaB protein in initiation of DNA replication, *J. Biol. Chem. 276*, 44919−44925.
9. Wahle, E., Lasken, R. S., and Kornberg, A. (1989) The dnaB−dnaC Replication Protein Complex of *Escherichia coli*. I. Formation and Properties, *J. Biol. Chem. 264*, 2463−2468.

10. Wahle, E., Lasken, R. S., and Kornberg, A. (1989) The dnaB-dnaC Replication Protein Complex of *Escherichia coli*. II. Role of the Complex in Mobilizing dnaB Functions, *J. Biol. Chem. 264*, 2469−2475.
11. Allen, G. C., and Kornberg, A. (1991) Assembly of the primosome of DNA replication in *Escherichia coli*, *J. Biol. Chem. 268*, 19204−19209.
12. Galletto, R., Rajendran, S., and Bujalowski, W. (2000) Interactions of Nucleotide Cofactors with the *Escherichia coli* Replication Factor DnaC Protein, *Biochemistry 39*, 12959−12969.
13. Galletto, R., and Bujalowski, W. (2002) The *Escherichia coli* Replication Factor DnaC Protein Exists in Two Conformations with Different Nucleotide Binding Capabilities. I. Determination of the Binding Mechanism Using ATP and ADP Fluorescent Analogs, *Biochemistry 41*, 8907−8920.
14. Galletto, R., and Bujalowski, W. (2002) Kinetics of *E. coli* Replication Factor DnaC Protein-Nucleotide Interactions. II. Fluorescence Anisotropy and Transient Dynamic Quenching Stopped-Flow Studies of the Reaction Intermediates, *Biochemistry 41*, 8921−8934.
15. Galletto, R., Jezewska, M. J., and Bujalowski, W. (2003) Interactions of the *Escherichia coli* DnaB helicase hexamer with the replication factor the DnaC protein. Effect of nucleotide cofactors and the ssDNA on the protein−protein interactions and the topology of the complex, *J. Mol. Biol. 329*, 441−465.
16. Hiratsuka, T., and Uchida, K. (1973) Preparation and properties of 2′(or3′)-*O*-(2,4,6-trinitrophenyl)adenosine 5′-triphosphate, an analog of adenosine triphosphate, *Biochim. Biophys. Acta 320*, 635−647.
17. Hiratsuka, T. (1983) New ribose-modified fluorescent analogs of adenine and guanine nucleotides available as substrates for various enzymes, *Biochim. Biophys. Acta 742*, 496−508.
18. Bujalowski, W., and Klonowska, M. M. (1993) Negative Cooperativity in the Binding of Nucleotides to *Escherichia coli* Replicative Helicase DnaB Protein. Interactions with Fluorescent Nucleotide Analogs, *Biochemistry 32*, 5888−5900.
19. Bujalowski, W., and Klonowska, M. M. (1994) Structural Characteristics of the Nucleotide Binding Site of the *E. coli* primary replicative Helicase DnaB Protein. Studies with Ribose and Base-Modified Fluorescent Nucleotide Analogs, *Biochemistry 33*, 4682−4694.
20. Bujalowski, W., and Klonowska, M. M.; Jezewska M. J. (1994) Oligomeric Structure of *Escherichia coli* Primary Replicative Helicase DnaB Protein, *J. Biol. Chem. 269*, 31359−31371.
21. Jezewska, M. J., Kim, U.-S., and Bujalowski, W. (1997) Interactions of *Escherichia coli* Primary Replicative Helicase DnaB Protein with Nucleotide Cofactors, *Biophys. J. 71*, 2075−2086.
22. Edelhoch, H. (1967) Spectroscopic determination of tryptophan and tyrosine in proteins, *Biochemistry 6*, 1948−1954.
23. Gill, S. C., and von Hippel, P. H. (1989) Calculation of protein extinction coefficients from amino acid sequence data, *Anal. Biochem. 182*, 319−326.
24. Azumi, T., and McGlynn, S. P. (1962) Polarisation of the Luminescence of Phenantrene, *J. Chem. Phys. 37*, 2413−2420.
25. Lakowicz, J. R. (1999) in *Principle of Fluorescence Spectroscopy*, pp 367−443, Plenum Press, New York.
26. Jezewska, M. J., Rajendran, S., and Bujalowski, W. (1998) Complex of *Escherichia coli* Primary Replicative Helicase DnaB Protein with a Replication Fork. Recognition and Structure, *Biochemistry 37*, 3116−3136.
27. Jezewska, M. J., and Bujalowski, W. (1996) Global Conformational Transitions in *E. coli* Primary Replicative DnaB Protein Induced by ATP, ADP and Single-Stranded DNA Binding, *J. Biol. Chem. 271*, 4261−4265.
28. Jezewska, M. J., Rajendran, S., and Bujalowski, W. (1998) Transition Between Different Binding Modes In Rat DNA Polymerase β − ssDNA Complexes, *J. Mol. Biol. 284*, 1113−1131.
29. Stafford, W., III. (1992) Boundary analysis in sedimentation transport experiments: a procedure for obtaining sedimentation coefficient distributions using the time derivative of the concentration profile, *Anal. Biochem. 203*, 295−301.
30. Correia, J. J., Chacko, B. M., Lam, S. S., and Lin, K. (2001) Sedimentation studies reveal a direct role of phosphorylation in Smad3: Smad4 homo- and hetero-dimerization, *Biochemistry 40*, 1473−1482.
31. Tanford, C. (1961) *Physical Chemistry of Macromolecules*, pp 364−390, John Wiley & Sons, Inc., New York.
32. van Holde, K. E., Johnson W. C., and Ho, P. S. (1998) in *Principle of Physical Biochemistry*, pp 192−241.
33. Cantor, C. R., and Schimmel, P. R. (1980) in *Biophysical Chemistry*, Part II, pp 591−641, W. H. Freeman and Company, New York.
34. Nakayama, N., Arai, N., Bond, M. W., Miyajima, A., Kobori, J., and Arai, K. (1987) Structure of *Escherichia coli* dnaC. Identification of a Cysteine Residue Possibly Involved in Association with dnaB Protein, *J. Biol. Chem. 262*, 10475−10480.
35. Lee, J. C., and Timasheff, S. N. (1979) The Calculation of Partial Specific Volumes of Proteins in 6 M Guanidine Hydrochloride, *Methods Enzym. 61*, 49−57.
36. Kuntz, I. D. (1971). Hydration of Macromolecules. III. Hydration of Polypeptides, *J. Am. Chem. Soc. 93*, 514−515.
37. Bull, H. B., and Breese, K. (1968) Protein Hydration. I. Binding Sites. *Arch. Biochem. Biophys. 128*, 488−496.
38. Bujalowski, W., Klonowska, M. M., and Jezewska, M. J. (1994) Close Proximity of Tryptophan Residues and ATP-binding Site in *Escherichia coli* Primary Replicative Helicase DnaB Protein, *J. Biol. Chem. 269*, 31350−31358.
39. Steiner, R. F. (1991) in *Topics in Fluorescence Spectroscopy*, pp 1−52, J. R. Lakowicz Ed., Plenum Press, New York.
40. Ware, W. R. (1980) in *Time-resolved Fluorescence Spectroscopy in Biochemistry and Biology* (Cundall, R. B., and Dale, R. E., Eds.) pp 299−317, Plenum Press, New York.
41. Mendelson, R., and Cheung, P. H−C. (1978) Intrinsic Segmental Flexibility of the S-1 Moiety of Myosin Using Single-Headed Myosin, *Biochemistry, 17*, 2139−2148.
42. Kobori, J. A., and Kornberg, A. (1982) The *Escherichia coli* dnaC Gene Product. I. Overproduction of the dnaC Proteins of *Escherichia coli* and *Salmonella Typhimurium* by Cloning into a High Copy Number Plasmid, *J. Biol. Chem. 257*, 13757−13762.
43. Kobori, J. A., and Kornberg, A. (1982) The *Escherichia coli* dnaC Gene Product. II. Purification, Physical Properties, and Role in Replication, *J. Biol. Chem. 257*, 13763−13769.
44. Barcena, M., Ruiz, T., Donate, L. E., Brown, S. E., Dixon, N. E., Radermacher, M., and Carazo, J. M. (2001) The DnaB-DnaC complex: a structure based on dimers assembled around an occluded channel, *EMBO J. 20*, 1462−1468.
45. Yu, X., Jezewska, M. J., Bujalowski, W., and Egelman, E. H. (1996)The Hexameric *E. coli* DnaB Helicase can Exist in Different Quaternary States, *J. Mol. Biol. 259*, 7−14.
46. Yang, S., Yu, X., VanLoock, M. S., Jezewska, M. J., Bujalowski, W., and Egelman, E. H. (2002) Flexibility of the Rings: Structural Asymmetry in the DnaB Hexameric Helicase, *J. Mol. Biol. 321*, 839−849.
47. Brochon, J. C., and Wahl, P. (1975) Measure des declines de l'anisotropie de fluorescence de la γ-globuline et de ses fragments Fab, Fc et $F(ab)_2$ marques avec le 1-sulfonyl-5-dimethyl-aminonaphthalene, *Eur. J. Biochem. 25*, 20−32.
48. Wahl, P. (1980) in *Time-Resolved Fluorescence Spectroscopy in Biochemistry and Biology* (Cundall, R. B., and Dale, R. E. Eds.) pp 483−495, Plenum Press, New York.
49. Tao, T. (1969) Time-Dependent Fluorescence Depolarization and Brownian Rotational Diffusion Coefficients of Macromolecules, *Biopolymers 8*, 609−632.
50. Norris, L., and Steiner R. F. (1987) Fluorescence Dynamics Studies of Troponin C, *Biopolymers 26*, 1189−1204.

BI049377Y